Effects of soluble guanylyl cyclase activation on skeletal muscle microcirculatory oxygen exchange in rats with heart failure with reduced ejection fraction

by

Ramona Elaine Weber

B.S., Kansas State University, 2019

A THESIS

submitted in partial fulfillment of the requirements for the degree

MASTER OF SCIENCE

Department of Kinesiology
College of Health and Human Sciences

KANSAS STATE UNIVERSITY
Manhattan, Kansas

2020

Approved by:

Co-Major Professor
David C. Poole, Ph.D., D.Sc.

Approved by:

Co-Major Professor
Timothy I. Musch, Ph.D.

Copyright

Abstract

Introduction: In heart failure (HF), nitric oxide (NO) pathway dysfunction impairs muscle arteriolar vasodilation and thus capillary hemodynamics, contributing to impaired oxygen uptake ($\dot{V}O_2$) kinetics. Due to poor prognosis and enhanced muscle fatigability following myocardial infarction, new treatment options are pursued heavily. To target downstream effects of NO directly, soluble guanyl cyclase (sGC) activators were developed. This investigation tested the hypotheses that chronic administration of a sGC activator would increase the O_2 delivery ($\dot{Q}O_2$)-to-O_2 utilization ($\dot{V}O_2$) ratio in the skeletal muscle interstitial space (PO_2*is*) of HF rats during twitch contractions due, in part, to increases in red blood cell (RBC) flux (f_{RBC}) and hematocrit (Hct_{cap}). Furthermore, we investigated whether exogenous NO (sodium nitroprusside, SNP) superfusion in addition to sGC activator would improve the $\dot{Q}O_2$-$\dot{V}O_2$ ratio and capillary hemodynamics further. **Methods:** HF was induced in adult male Sprague-Dawley (3-4 mo. old) rats via myocardial infarction (MI). Following ~3 weeks of HF progression, 0.3 mg/kg sGC activator in 1 ml vehicle (10% Transcutol, 20% Cremophor, Sigma Aldrich, St. Louis, MO, and 70% water) was administered via oral gavage twice a day (HF + sGC; n =10) for 5 days prior to phosphorescence quenching (PO_2*is*, in contracting muscle) and intravital microscopy (rest) measurements in the spinotrapezius muscle. The control heart failure group (HF; n = 9) received vehicle only. Intravital microscopy measured f_{RBC}, V_{RBC}, and Hct_{cap} under resting conditions. **Results:** Intravital microscopy revealed greater increases in Hct_{cap} (+16 ± 1 vs 10 ± 1%) of HF + sGC vs HF, respectively. Interestingly, f_{RBC} and V_{RBC} respectively, were both increased in HF + sGC vs HF (70 ± 9 vs 25 ± 8 RBC/s) and (490 ± 43 vs 226 ± 35 μm/s) ($P < 0.05$). A greater number of capillaries supporting flow was seen in HF + sGC (91 ± 3 vs 82 ± 3%, $P < 0.10$). f_{RBC} and V_{RBC} were strongly correlated ($r = 0.958$). During 14-22 seconds of contractions there was an

increase in PO_2*is* in HF + sGC vs HF ($P \leq 0.05$). **Conclusions:** Our findings suggest that increased resting $\dot{Q}O_2$ via f_{RBC}, V_{RBC}, and Hct_{cap} allow for better $\dot{Q}O_2$-to-$\dot{V}O_2$ matching, reversing a likely limitation to HF, while also avoiding pernicious interactions with reactive oxygen species or tolerances experienced with NO supplementation. Additionally, during the rest-contraction transient, sGC activator increases PO_2*is*, which may speed $\dot{V}O_2$ kinetics. Together, our findings support that sGC activators as a potential therapeutic targeting vasomotor dysfunction in HF which would be expected to increase exercise capacity by speeding $\dot{V}O_2$ kinetics.

Table of Contents

List of Figures

List of Tables

Acknowledgements

I would like to acknowledge my mentors Dr. David Poole and Dr. Tim Musch for their everlasting inspiration, support, and commitment to helping me succeed and understand the scientific process, Dr. Steven Copp for his helpful insight pertaining to this study, and Dr. Carl Ade for his patience and love for echocardiography. I would like to thank Sue Hageman for her help with surgical preparations and early morning optimism, and Dr. Trenton Colburn for his guidance when I first expressed interest in research. Additionally, I would like to thank my lab mates Kiana Schulze, Dr. Trenton Colburn, and Andrew Horn for the support, the thought-provoking dialogues, and creating the best laboratory environment—I could not have asked for a better team.

Dedication

I would like to dedicate my thesis to several people who have helped me become the person I am today: my late aunt, Beatrice Weber, and late grandfather, Edward Sage, who taught me to persevere from a young age, my parents, Beth Owens and Marty Weber, for never underestimating me, my siblings, Juliet Weber, Sara Weber, Jenny Weber, Nolan Weber, Joanna Weber, and Jonah Weber for always believing in me and cheering me on, and lastly, my friend Madalyn Ellenbecker. Without this group of individualistic, strong people, none of this would've been possible.

Chapter 1 - Introduction

Heart failure with reduced ejection fraction (HF) imposes an extensive health care burden (~30 million patients worldwide) despite the use of guideline-based medical therapies such as angiotensin-converting enzyme inhibitors, angiotensin receptor blockers, mineralocorticoid-receptor antagonists, and beta-blockers (Butler et al., 2019*).* Therefore, novel pharmacological interventions are critical to overcome persistent poor prognoses and improve exercise capacity. HF is a multifaceted disease characterized by a decrease in cardiac output consequent to diminished stroke volume and ejection fraction (i.e., impaired contractility) (Abraham et al*.*, 2003, La Rovere et al., 2003), chronic sympathetic activation resulting in reduced peripheral perfusion (Drexler et al., 1992a, Musch et al., 1992, Kindig et al., 1999, Richardson et al., 2003, Hillege et al., 2000), and perturbations in metabolic function (Massie et al., 1988).

Exercise intolerance is a cardinal manifestation of HF, owing, in large part, to diminished perfusive and diffusive oxygen (O_2) transport (Poole et al., 2012, 2018, Piepoli et al., 2014). At the onset of exercise, the delivery of O_2 ($\dot{Q}O_2$) needs to match the demand of O_2 utilization ($\dot{V}O_2$). However, impaired capillary hemodynamics compromises the dynamic matching between $\dot{Q}O_2$-to-$\dot{V}O_2$ and decreases muscle microvascular oxygenation (PO_2*mv*, interstitial PO_2, PO_2*is*) during transitions in metabolic demand, i.e. the onset of exercise (Diederich et al., 2002, Richardson et al., 2003, Craig et al., 2019a*).* A reduction in skeletal muscle mass, increase in percentage of type II fibers, with a decrease of type I fibers, and muscle atrophy likely exacerbate the inability to exercise in this disease state. Importantly, HF rats (induced by a surgically induced myocardial infarction, MI) exhibit a significant decrease in PO_2*is* (the pressure driving O_2 into the contracting myocyte) in skeletal muscle at rest and during electrically induced contractions when compared to healthy control animals (Craig et al., 2019a),

thus diminishing the O_2 available to the skeletal muscle and altering metabolic control (i.e., driving glycolysis, accumulation of fatigue-related metabolites) (Hirai et al., 2018, Massie et al., 1987). Furthermore, the capillary vascular bed (the largest surface area for O_2 exchange in the skeletal muscle microvascular network) is a limiting factor to exercise capacity at least in HF rats post-MI. Specifically, resting capillary hemodynamics evince a 45-55% decrease in red blood cell (RBC) velocity (V_{RBC}) and flux (f_{RBC}) when compared to healthy control rats (Kindig et al., 1999), indicative of decreased $\dot{Q}O_2$. A decreased O_2 diffusing capacity (DO_2) in HF rats stems from lower HCT_{cap} and decreased proportion of capillaries supporting f_{RBC}, which further attenuates oxidative function of the skeletal muscle. Given the role of skeletal muscle dysfunction in HF, the importance of capillary hemodynamic control, and PO_2*is*, a better understanding of the mechanistic bases for improving muscle function in HF is imperative to better develop effective therapeutic countermeasures.

Endothelial dysfunction contributes to the exercise intolerance seen in patients with HF and HF rats due, in part, to reduced nitric oxide (NO) bioavailability, a critical signaling molecule in vascular homeostasis and control of the exercise hyperemia (Ferreira et al., 2006). Diminished production of NO or its scavenging by reactive oxygen species (ROS) (Cai & Harrison, 2000) results in inactivation of soluble guanyl cyclase (sGC), the enzyme responsible for converting guanosine triphosphate (GTP) to cyclic guanosine monophosphate (cGMP) which results in increased intracellular calcium and vasoconstriction, ultimately causing a blunted hyperemic response to exercise (Hirai, et al., 1995). The pharmacological properties of NO, namely, increased vasodilation and decreased platelet aggregation, remodeling, apoptosis, and inflammation, have been exploited for over a century in an effort to reduce ischemia associated with cardiovascular disease (Brunton et al., 1897). Organic nitrates, such as nitroglycerin, have

potent acute vasodilatory effects in HF (Daiber & Münzel, 2015), which improve symptoms such as angina associated with HF. In order to restore NO bioavailability, therapies based on inorganic nitrates, such as beetroot juice, have been implemented and shown to improve blood flow, oxygenation, and thus metabolic control within the exercising muscles (Ferguson et al., 2016). However, the efficacy may be limited due to development of tolerance following prolonged administration (Elkayam, et. Al., 1987; Munzel et al., 2011) especially with organic nitrates and/or the occurrence of tachyphylaxis, which is associated with an increased generation of superoxide, O_2^- , contributing to cardiovascular disease progression (Munzel et al., 1995, Warnholtz, et al., 2002). Therefore, downstream targets of the NO pathway may prove invaluable as a means to avoid O_2^- production in HF. Recent therapies have focused on sGC via sGC activators, a novel therapeutic synthesized to target pathological sGC, to elicit vascular smooth muscle relaxation in disease conditions such as pulmonary hypertension, liver fibrosis, renal damage, erectile dysfunction, and fibrotic diseases (Pankey et al., Knorr et al., 2008, Benz et al., Silva et al., 2014, Irvine et al., 2012).

sGC activators increase the catalytic activity of oxidized (pathological) sGC and promote vasodilation in experimental models where NO donors are rendered inactive (Pankey et al., 2011, Fraccarollo et al., 2014). In isolated smooth muscle cells of diseased versus healthy blood vessels, sGC activators have greater pharmacological activity by inducing endothelium-independent smooth muscle vasodilation, thereby demonstrating the potential for improving skeletal muscle oxygenation and improved capillary hemodynamics in HF (Stasch et al., 2006). What remains unknown is if sGC activators are capable of modulating O_2 delivery within the interstitial space through increased PO_2*is* and increased $\dot{Q}O_2$ via improved capillary V_{RBC}, f_{RBC}, and DO_2 by elevated capillary hematocrit (Hct_{cap}). Therefore, to assess the utility of sGC

activators in the skeletal muscle of HF rats, this investigation tested the hypotheses that chronic administration of a sGC activator would improve $\dot{Q}O_2$-to-$\dot{V}O_2$ matching in the skeletal muscle (i.e., increase PO_2*is*) of HF rats during contractions due, in part, to increases in the proportion of capillaries flowing and elevated Hct_{cap}, f_{RBC}, and V_{RBC} in those capillaries. Furthermore, we investigated whether a ceiling effect of sGC activation was present, or, alternatively, whether exogenous NO (sodium nitroprusside, SNP) superfusion in addition to sGC activation would further improve skeletal muscle oxygenation.

Chapter 2 - Methods

Animals

All procedures were approved by the Institutional Animal Care and Use Committee of Kansas State University and conducted according to the National Research Council *Guide for the Care and Use of Laboratory Animals.* Experiments were performed on 19 male Sprague-Dawley rats (3-4 mo old, Charles River Laboratories, Wilmington, MA). Upon arrival, animals were maintained in accredited (Association for the Assessment and Accreditation of Laboratory and Animal Care; AAALAC) animal facilities under a 12:12 h light:dark cycle with food and water provided *ad libitum*.

Myocardial Infarction Procedure

A MI was induced via surgical ligation of the left main coronary artery (Musch & Terrell, 1992). Initially, rats were anaesthetized with 5% isoflurane-O_2 mixture and intubated for mechanical ventilation with a rodent respirator (model 680, Harvard Instruments, Holliston, MA) for the duration of the surgical procedure. The heart was exposed through a left thoracotomy in the fifth intercostal space. The left main coronary artery was ligated with 6-0 silk suture ~1-2 mm distal to the edge of the left atrium. The incision was closed and ampicillin (50 mg kg^{-1} i.m.) was injected locally to reduce susceptibility to infection. The analgesic agents bupivacaine (1.5 mg kg^{-1} s.c.) and buprenorphine (0.01-0.05 mg kg^{-1} i.m.) were administered and anesthesia and mechanical ventilation discontinued. All rats were monitored closely for ~6 h for arrhythmia development and signs of stress with care administered as appropriate according to an intensive

10-day post-operative plan conducted in conjunction with the university veterinary staff. Rats were assessed daily for signs of distress (appetite, weight loss/gain, gait/posture, etc.)

Echocardiography

21 days following MI, confirmatory echocardiography was performed to assess left ventricular (LV) function. As previously described (Craig et al., 2019a), transthoracic echocardiography was performed using a commercially available system (Logiq S8; GE Health Care, Milwaukee, WI) with an 18 MHz linear transducer (L8-18i). Rats were initially anesthetized with a 5% isoflurane-O_2 mixture and placed on a heating pad to maintain core temperature. Standard two-dimensional and M-mode images from the midpapillary level were obtained with frame rates of >50 frames/s. Ventricular dimensions and wall thicknesses were obtained from M-mode measurements over four consecutive cardiac cycles. LV internal dimensions and posterior wall (PW) thicknesses were measured at end systole (LVID; PWs) and end diastole (LVIDd; PWd) Fractional shortening (FS) was calculated from the measurements of LV chamber diameters: FS= [(LVIDd – LVIDs)/LVIDd] × 100. Left end-systolic (LVESv) and end-diastolic (LVEDv) volumes were calculated using the Teichholz formula: LV volume = (7.0/2.4 + LV dimension) × LV dimension^3. Stroke volume was calculated as: SV = LVEDv- LVESv. Ejection fraction (EF) was calculated as: EF = [LVEDv- LVESv/LVEDv] × 100.

Drug Dosing

Following echocardiography, rats were randomly assigned to heart failure (HF; n = 9) or activator (HF + sGC; n = 11) groups. The sGC activator was administered via oral gavage. The sGC activator was weighed and mixed with 10% Transcutol, 20% Cremophor, (Sigma Aldrich,

St. Louis, MO), and 70% water to obtain a dose with the final concentration of 0.3 mg/kg sGC activator in a 1ml volume. The HF group was given solvent only. To mimic clinical protocols, the drug was administered in the ACT group b.i.d. for 5 days prior to the following experimentation.

Surgical Preparations

Following dosing protocols, rats were anaesthetized initially with a 5% isoflurane-O_2 mixture and subsequently maintained at 2-3% isoflurane-O_2 while positioned on a heating pad to maintain core temperature at ~37-38℃, measured via rectal thermometer. The carotid artery was isolated and cannulated and a 2-French catheter-tip pressure transducer (Millar Instruments, Houston, TX, USA) was advanced into the LV for measurements of systolic and diastolic pressures and LV delta pressure/delta time (LV d*p*/d*t*). Upon completion of the LV measurements, the transducer was removed, and the carotid artery was re-cannulated with a catheter (PE-10 connected to PE-50, Intra-Medic polyethylene tubing, Clay Adams Brand, Benton, Dickson and Company, Sparks, MD, USA) for measurement of mean arterial pressure (MAP) and heart rate (HR). A second catheter was introduced into the caudal artery for administration of pentobarbital sodium anesthesia and arterial blood sampling. Rats were then progressively transitioned from isoflurane onto pentobarbital sodium anesthesia (0.02-0.05 ml doses diluted in ~.3 ml of heparinized saline). Depth of anesthesia was continuously monitored via toe pinch and corneal responses with pentobarbital sodium administered throughout the remaining experimental protocols.

The overlying skin and fascia were carefully removed from the mid-dorsal-caudal region of the rat. The right spinotrapezius muscle was exposed in a manner that did not disrupt vascular

supply to the muscle (Bailey et al., 2000). Importantly, this muscle was used due to its similar fiber-type composition of the human untrained quadriceps muscle (Delp & Duan, 1996). Silver wire electrodes were then sutured (6-0 silk) to the rostral (cathode) and caudal (anode) regions of the muscle to induce twitch contractions. The exposed muscle was continuously superfused with Krebs-Henseleit bicarbonate-buffered solution (4.7mM KCl, 2.0 mM $CaCl_2$, 2.4 mM $MgSO_4$, 131 mM NaCl, and 22 mM $NaHCO_3$; pH= 7.4; equilibrated with 5% CO_2-95% N_2 at 38℃) and the surrounding tissue was covered with Saran Wrap (Dow Industries, Indianapolis, IN) to minimize dehydration.

Experimental Protocol

Following the surgical preparation, phosphorescence quenching determined the partial pressure of oxygen in the interstitial space of the muscle (PO_2*is*) at rest and during contractions using a frequency domain phosphorimeter (PMOD 500; Oxygen Enterprises, Philadelphia, PA) as previously described (Craig et al., 2019b; Colburn et al., 2020; Hirai et al., 2018, 2019). To minimalize any phosphorescent interference, all measurements were performed in a dark room with minimal light exposure. Oxyphore G4 (Pd-*meso*-tetra-(3,5-dicarboxyphenyl)-tetrabenzo-porphyrin) was injected locally into the muscle (3-4 10μL injections at 10-μM concentration) using a 29-G needle. Care was taken to avoid damaging any visible vasculature. This probe allows dynamic visualization of the tissue PO_2*is* levels of the spinotrapezius muscle (Esipova et al., 2011). Following injections, the spinotrapezius muscle was covered with Saran wrap to protect the muscle from dehydration during a 15-minute period which allows for diffusion of G4 throughout the muscle in the interstitial space. A bifurcated light guide was positioned ~3-4 mm above the surface of the exposed muscle in a field absent of large vessels. Twitch contractions

were electrically evoked (1Hz, 6-7 V, 2-ms pulse duration) with a Grass S88 Stimulator (Quincy, MA) for 180 s. This contraction protocol increases spinotrapezius muscle blood flow ~5 fold and the metabolic rate ~7 fold without altering blood pH. This is consistent with moderate-intensity exercise (Behnke et al., 2002) and elicits highly reproducible responses (Craig et al., 2019a; Colburn et al., 2020; Hirai et al., 2018). PO_2*is* was then measured and recorded at 2s intervals throughout the duration of the protocol. Following the first contraction protocol (CON), 20 minutes were allowed for the muscle to fully recover before the experiment was repeated. In the second contraction protocol the spinotrapezius was superfused with the NO donor sodium nitroprusside (SNP; 300 µM) before contractions to determine responses between HF + sGC and HF groups. The light guide remained in the exact same position as for the first contraction protocol.

Analysis of Interstitial PO_2 Kinetics

The kinetic analyses of PO_2*is* response was measured using 10 s of resting data prior to the 180-s contraction bout utilizing the Stern-Volmer relationship and using a monoexponential plus time delay model:

$$PO_2\ (t) = PO_{2(BL)} - \Delta_1 PO_2[1-e^{-(t-TD)/\tau}]$$

or a monoexponential plus time delay using a secondary component when required:

$$PO_2\ (t) = PO_{2(BL)} - \Delta_1 PO_2[1-e^{-(t-TD)/\tau}] + \Delta_2 PO_2[1-e^{-(t-TD)/\tau^2}]$$

where PO_2 (t) represents the PO_2*is* at any point in time, $PO_{2\ (BL)}$ is the baseline before the onset of contractions, Δ_1 and Δ_2 are the primary and secondary amplitudes, TD and TD_2 are the time delays for each component, and τ and τ^2 are the time constants (i.e., the time required to reach 63% of the amplitude) for the primary and secondary amplitudes. The mean response time was

calculated as the sum of the model-derived TD and τ. When the secondary component model was necessary, the primary amplitude was constrained to not exceed the nadir value to maximize accuracy of the primary response kinetics. The goodness of model fit was determined using the following criteria: 1) the coefficient of determination; 2) sum of squared residuals; 3) visual inspection and analysis of the model fits to the data and the residuals. Since the second amplitude (Δ_2PO_2, undershoot of the PO_2) was often monoexponential in nature, it was manually calculated by subtracting the difference between the PO_2*is* at the end of contractions minus the nadir value of PO_2*is* during contractions.

Intravital Microscopy

Following PO_2*is* measurements, electrode sutures were gently removed. The caudal end of the spinotrapezius was carefully dissected and sutured (6-0 silk) to a thin wire horseshoe-shaped manifold at five-six equidistant points around the perimeter. The exposed dorsal surface of the muscle was protected with Saran Wrap to prevent dehydration. The rat was then placed on a water circulation-heated Lucite platform with the spinotrapezius positioned such that a microvascular field, midway between arteriolar and venular ends within the midcaudal dorsal surface, could be observed using an intravital microscope (Nikon, Eclipse E600-FN; ×40 objective; 0.8 numerical aperture) equipped with a noncontact, illuminated lens, and a high-resolution color monitor (total viewing area = 270 × 210 μm; Sony Trinitron PVM-1954Q, Ichinonya, Japan).The muscle was transilluminated to ensure clear resolution of the sarcomere A-bands within one-third to two-thirds of the muscle fibers. The final magnification (×1,184) was confirmed by initial calibration of the system using a stage micrometer (MA285, Meiji Techno). This magnification is adequate for measuring all essential structural and hemodynamic

variables (Poole et al., 1997; Kindig et al., 1999). The spinotrapezius muscle was maintained at physiological sarcomere length (~2.7 μm) throughout the subsequent observation period, and any exposed tissue was continuously superfused with the Krebs-Henseleit solution. Once the spinotrapezius muscle was positioned on the platform, 8–10 microvascular viewing fields were each recorded for ~1–1.5 min for every animal. Following initial recordings, SNP (300 μM) was superfused onto the muscle. Recordings were time referenced by frame and fields and stored for subsequent offline analysis. MAP was monitored continuously throughout the data-acquisition period.

Capillary Data Analysis

5-7 fields were chosen randomly from each rat for analysis on the basis of clear visualization of sarcomeres, fibers, and capillaries. Capillaries supporting RBC flow were assessed in real time, and each capillary was placed into one of two categories: 1) normal flow = 30 s of continuous, or 2) impeded flow or stopped flow for >10 of 30 s. These criteria were further used for determination of percentage of flowing capillaries [i.e., (number of capillaries supporting RBC flow/total number of visible capillaries per area) × 100]. For all capillaries in which hemodynamics were assessed and where the capillary endothelium was clearly visible on both sides of the lumen, capillary luminal diameter (dc) was measured (2–4 measurements /capillary) with calipers accurate to ± 0.25 mm (± 0.17 μm at ×1,184 magnification).

Examination of the microvascular fields was conducted in real time and by frame-by-frame analysis techniques (Dartfish Video Software, Fribourg, Switzerland) (30 frames/s). Sarcomere length was determined from sets of 10 consecutive in-register sarcomeres (i.e., distance between 11 consecutive A-bands) measured parallel to the muscle fiber longitudinal

axis. This measurement was repeated 3–4 times where sarcomeres were visible to obtain a mean sarcomere length for each viewing field. V_{RBC} was determined in all capillaries that were continuously RBC perfused by following the RBC path length over several frames. F_{RBC} was measured by counting the number of RBCs in a capillary passing an arbitrary point. For each capillary in which hemodynamic data were measured, capillary tube hematocrit (Hct_{cap}) was calculated by the following equation:

$$Hct_{cap} = (volume_{RBC} \times F_{RBC}) / [\pi \times (d_c/2)^2 \times V_{RBC}]$$

where $volume_{RBC}$ is RBC volume, which was taken to be 61 μm^3 (Altman & Dittmer, 1974) and capillaries were approximated as circular in cross section (Kindig et al., 1998). Following intravital microscopy the animals were killed with an overdose of pentobarbital sodium.

Heart Failure Classification

Left ventricular infarct size was determined by making an incision through the interventricular septum, from the base to the apex of the LV and a digital photograph of the endocardium was taken. The image was printed and infarct size determined by planimetry as previously described (Craig et al., 2019b).

Blood Sampling

MAP and HR were continuously measured during the experiment via right carotid artery connected to a pressure transducer and Digi-med Blood Pressure Analyzer (model 400; Micro-Med, Louisville, KY). Approximately 0.4 ml of blood was sampled from the caudal artery catheter at the end of the PO_2*is* measurements for the determination of arterial blood lactate

([La^-]), pH, P_{CO_2}, $\%O_2$ saturation, and systemic hematocrit (Nova Stat Profile M; Nova Biomedical, Waltham, MA).

Statistical Analysis

All PO_2*is* curve fitting and statistical analyses were performed using a commercially available software package (SigmaPlot 12.5, Systat Software, San Jose, CA). Student paired and unpaired t-tests were performed, when appropriate, to determine differences in morphometric, pressure, and microscopy measurements followed by Pearson correlation tests. A two-way analysis of variance (ANOVA) was used to detect differences in PO_2*is* kinetic parameters between HF + sGC and HF for CON and SNP conditions. A two-way repeated measures ANOVA was used to assess temporal interactions between HF + sGC and HF. Tukey's post hoc tests were used for multiple comparisons when significant differences were detected. Data are presented as means ± SE. Significance was accepted at $P < 0.05$.

Chapter 3 - Results

Morphometric Data

Twenty rats (HF + sGC, n = 11; HF, n = 9) were analyzed for morphometric and echocardiographic data. Body weight (BW) was reduced in the HF + sGC group compared to the HF group at final measurement (450 ± 11 g vs. 501 ± 14; $P \leq 0.01$, Table 1) despite no differences in age. Decreased LVDBP was seen in HF + sGC versus HF ($P < 0.05$, Table 1). Increased lung/BW was observed in the HF + sGC group ($P< 0.05$, Table 1), which may be attributed to the lower body mass, potentially due to reduced fluid retention. Measurements of LV function were assessed prior to dosing the rats via transthoracic echocardiography and post-experimentation via planimetry.

Echocardiographic Assessment

Infarct size did not differ between groups (Table 1). No differences were shown between groups in any echocardiographic measurements (fractional shortening; 20.5 ± 3.0 vs. 21.0 ± 2.9 %, ejection fraction; 44.7 ± 5.1 vs. 46.3 ± 4.8%; stroke volume; 0.8 ± 0.1 vs. 0.9 ± 0.1 ml/beat, HF + sGC vs HF, respectively; all $p > 0.05$).

RBC Hemodynamics

17 rats (HF; n = 8, HF + sGC; n = 9) were utilized for RBC hemodynamic measurements due to two animals losing hemodynamic stability. No differences were apparent between HF + sGC and HF + sGC SNP conditions. Sarcomere length was unchanged across groups and conditions, ranging from 2.4-2.5μm. Increased f_{RBC}, V_{RBC}, and Hct_{cap} were observed in HF + sGC vs both HF and HF SNP ($P < 0.01$). HF + sGC supported an increase in capillaries with flow (P

< 0.10). f_{RBC} and V_{RBC} had a positive correlation (R = 0.958) (Figure 5). The slope of this relationship dictates Hct_{cap}.

Phosphorescence Quenching

Nineteen rats were utilized for the SNP PO_2*is* measurements due to one not completing the protocol (HF + sGC n = 10; HF n = 9). There was a lower resting HR and LVDBP (Table 1, P < 0.05) in HF + sGC versus HF group despite no significant differences in MAP or HR during contractions. Following contractions there was a significant lower lactate concentration, but no blood gases or pH differences were observed (P > 0.05, Table 2).

Mean PO_2*is* profiles at rest and during contractions are presented in Figure 6. No significant differences were identified for the kinetics parameters between HF and HF + sGC groups during CON and SNP contractions (P > 0.05; Table 3). However, PO_2*is* values were lower in HF rats ($P \leq 0.05$, Figure 6A) during 14-22 seconds of CON contractions. No significant differences were observed in response to SNP superfusion (P > 0.05; Figure 7) between HF and HF + sGC. Contractions following SNP exhibited elevations in several PO_2 parameters: $PO_{2(BL)}$, $\Delta_1 PO_2$, τ, MRT, $PO_{2(Nadir)}$, $PO_{2(End)}$, and AUC in both HF + sGC and HF group (P < 0.001 vs CON, Table 3).

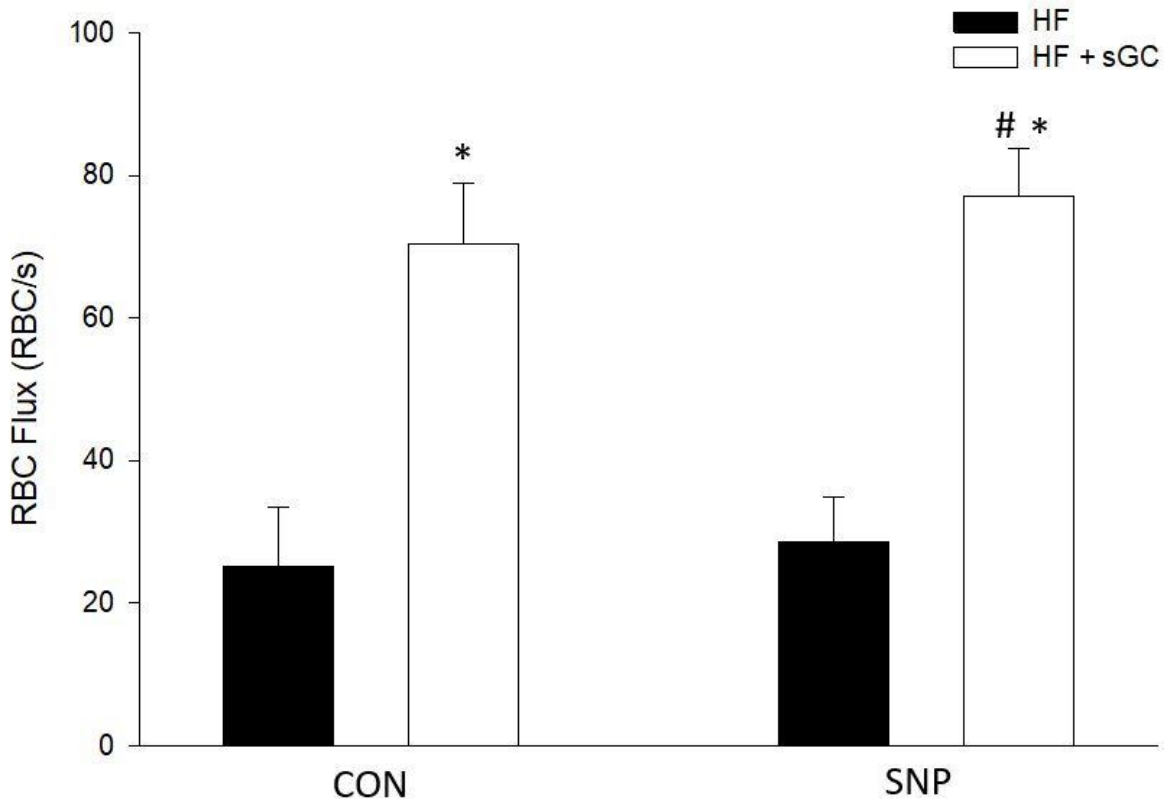

Figure 1: RBC flux. Group mean red blood cell (RBC) flux for CON and SNP conditions ± SE. * P < 0.01 vs HF CON. # P < 0.01 vs HF SNP. HF; closed bar, HF + sGC; open bar.

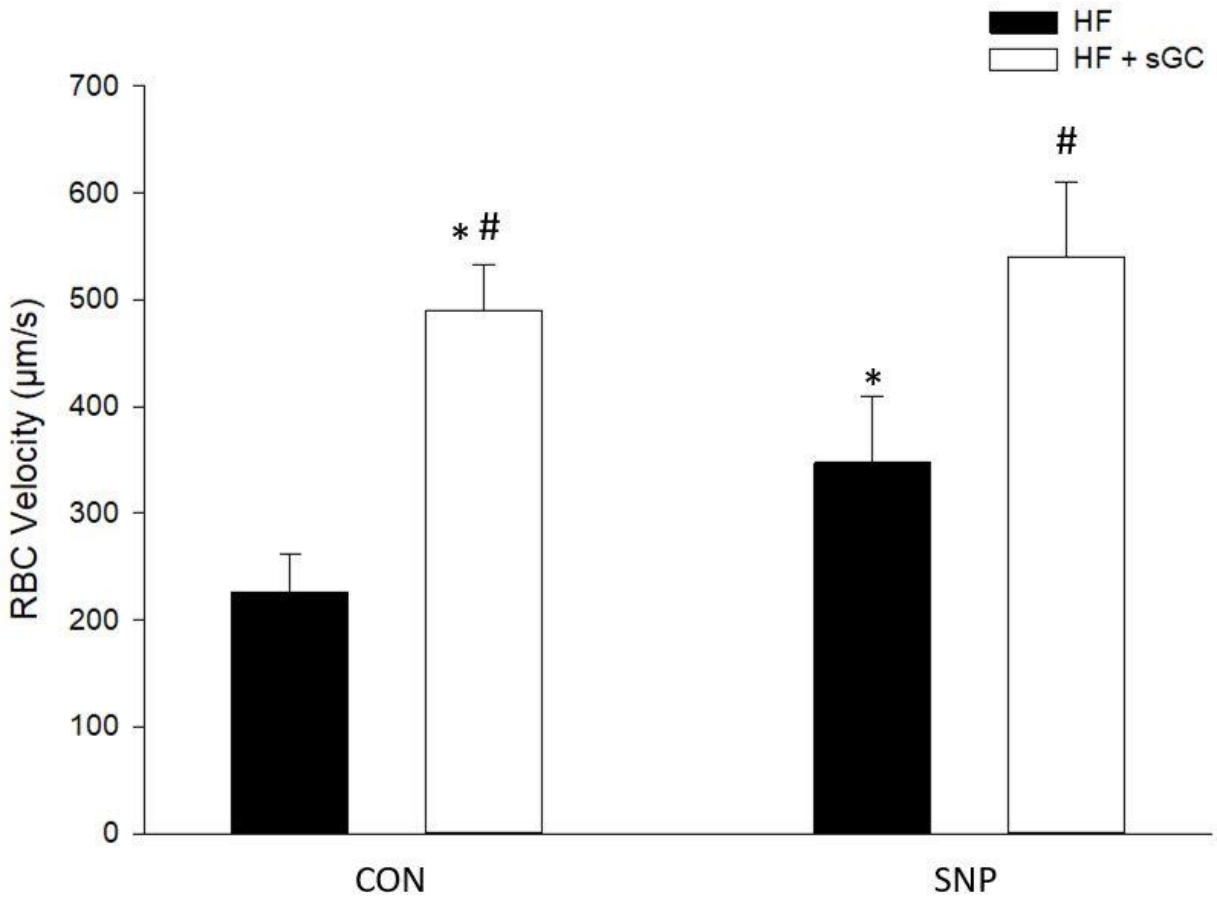

Figure 2: RBC velocity. Group mean red blood cell (RBC) velocity for control and SNP conditions ± SE. * $P < 0.05$ vs HF CON. # $P < 0.10$ vs HF SNP. HF; closed bar, HF + sGC; open bar.

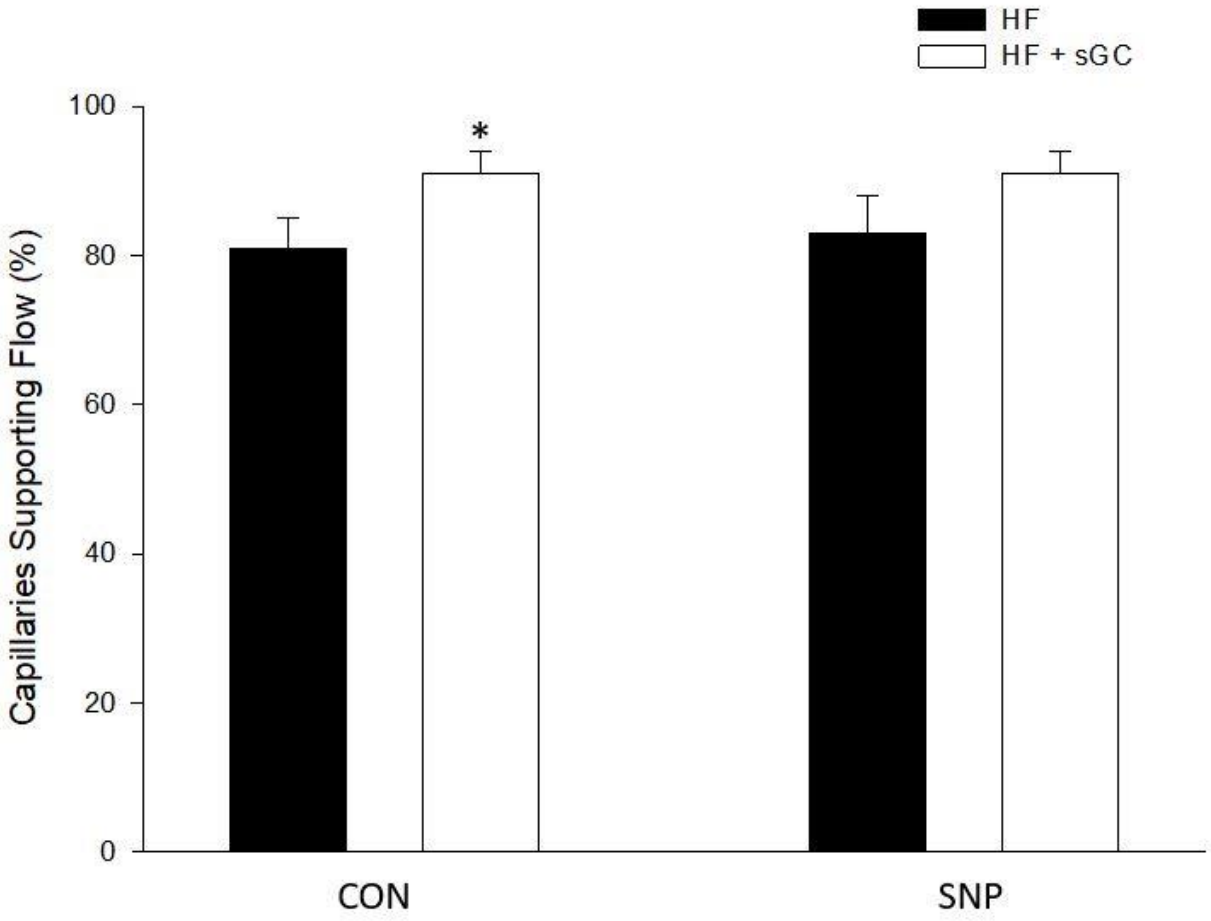

Figure 3: Percentage of capillaries supporting RBC flow. Percentage of capillaries supporting flow for control and SNP conditions ± SE. * P < 0.10 vs. HF CON.

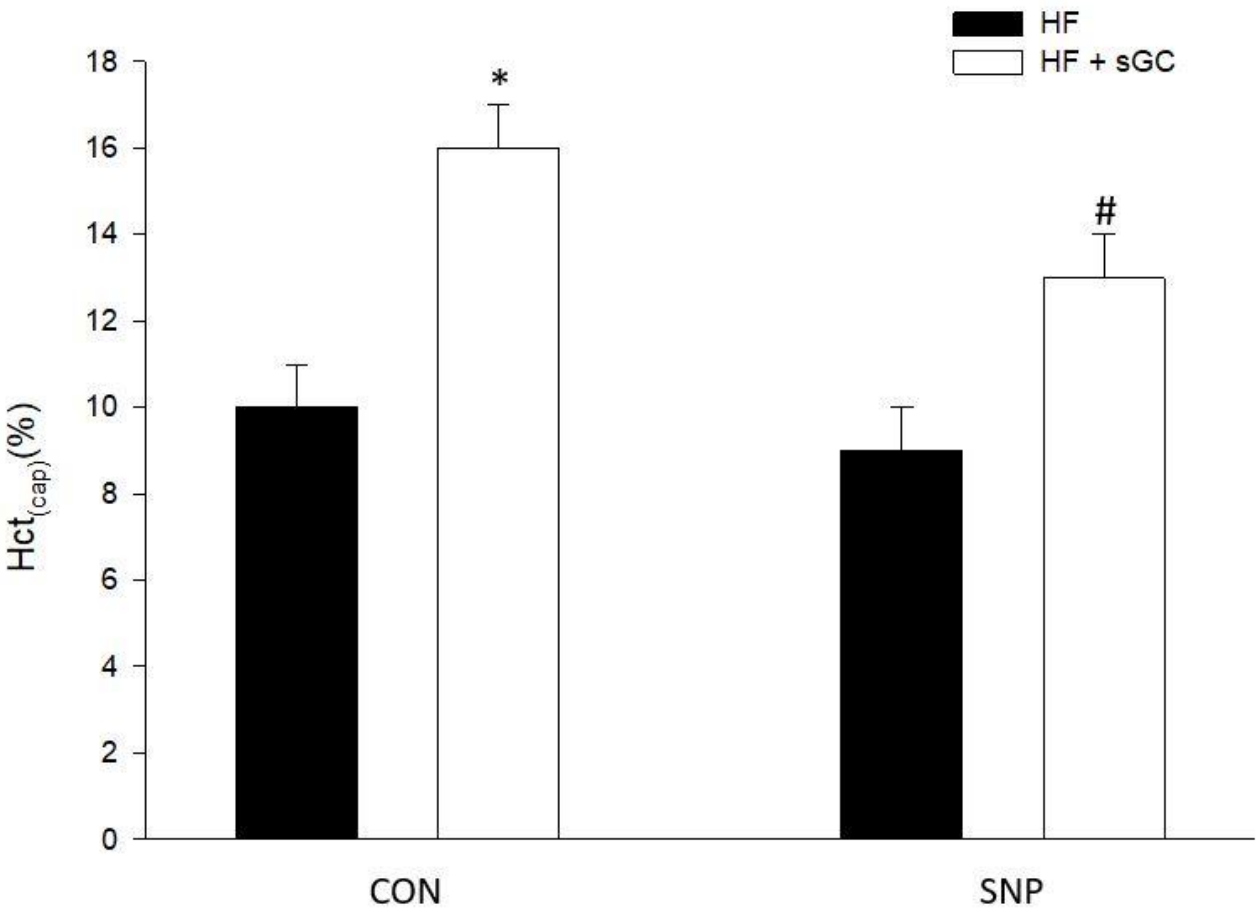

Figure 4: Capillary hematocrit. Capillary hematocrit, $Hct_{(cap)}$, ± SE. * P < 0.01 vs. HF CON. # P < 0.05 vs HF SNP.

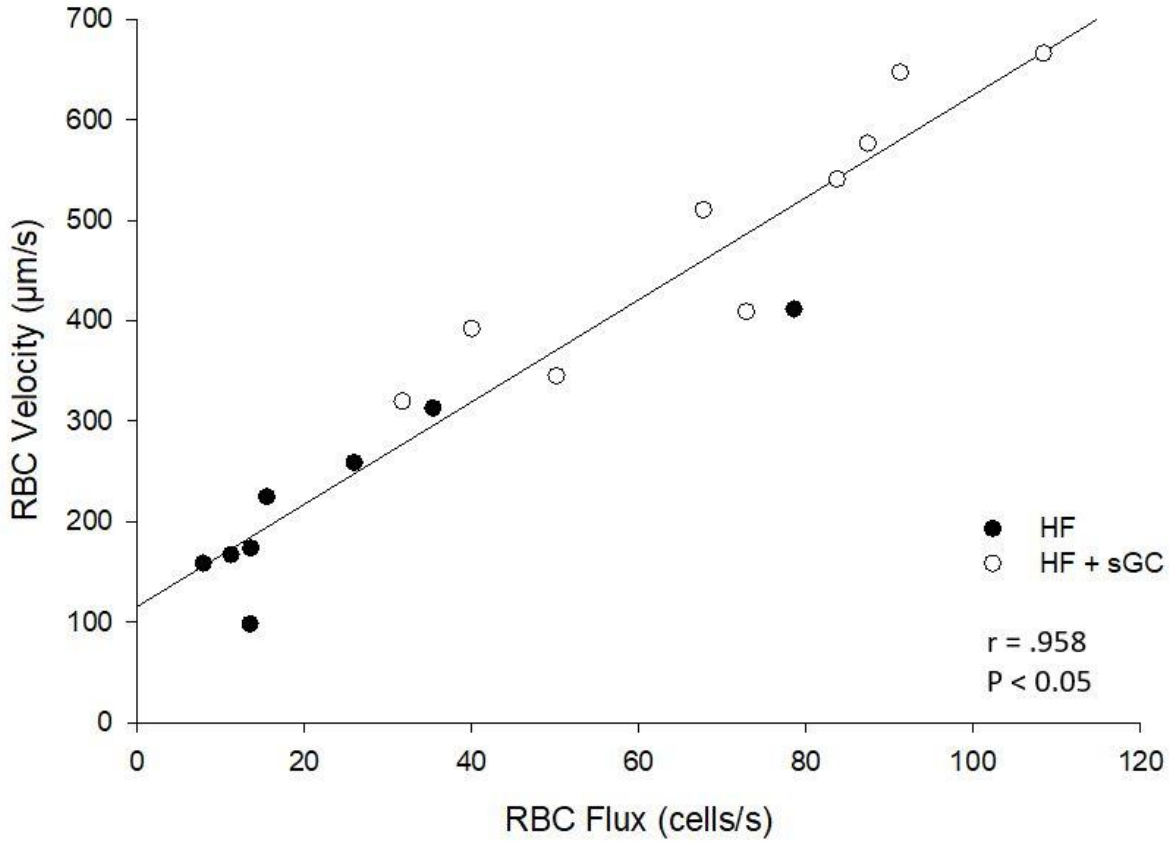

Figure 5: Relationship between RBC flux and velocity. A positive correlation (r = .958) is shown between RBC flux and RBC flux ($P < 0.05$). HF; closed circles, HF + sGC; open circles.

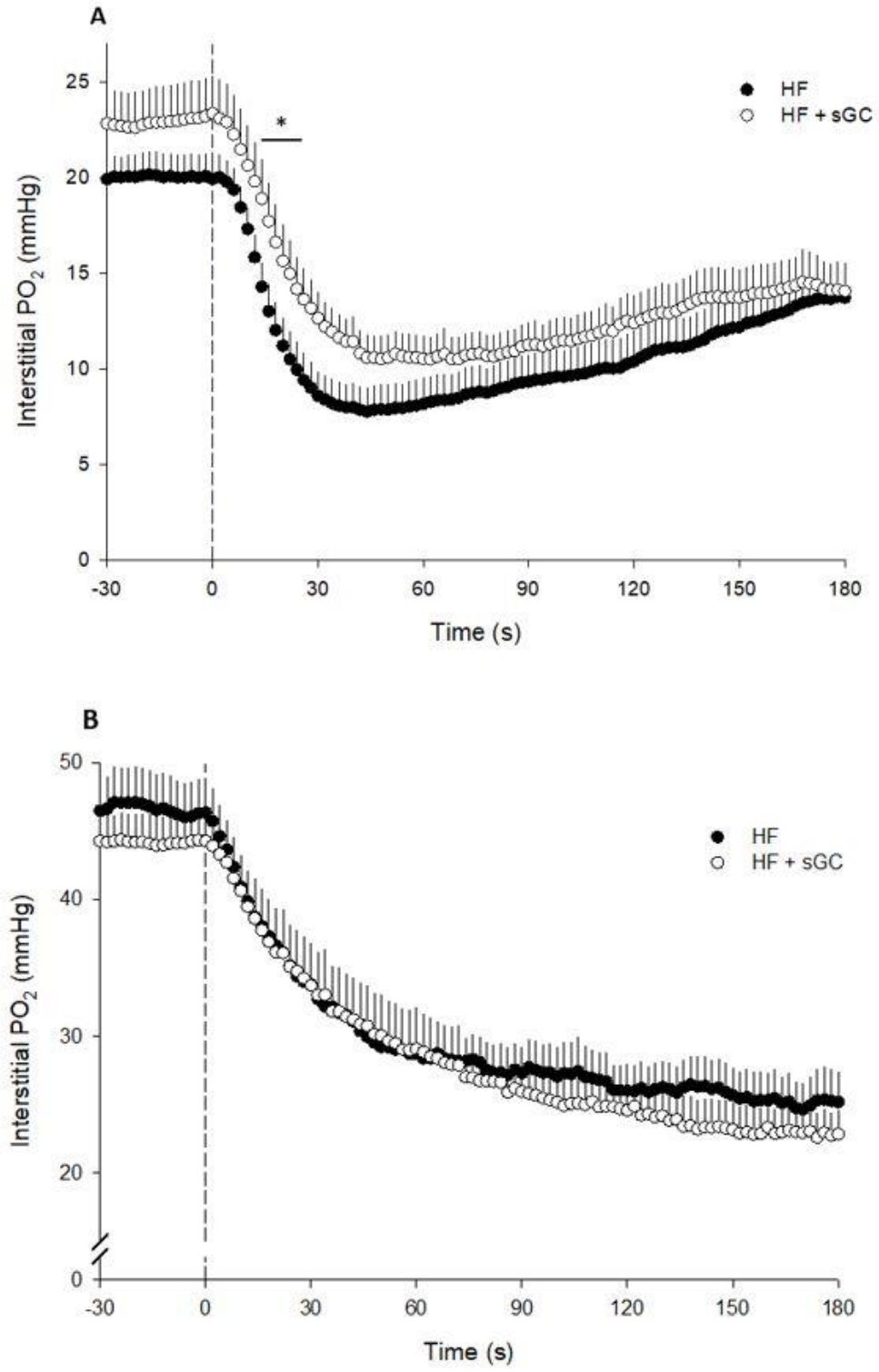

Figure 6: Interstitial PO_2 throughout contractions. Group mean (± SE) PO_2*is* dynamic profiles during 30 seconds of rest and 180 seconds of contractions. Dashed line indicates the onset of contractions. A: CON, 14-22 seconds * $P < 0.05$. B: SNP $P > 0.05$. HF; closed circles, HF + sGC; open circles.

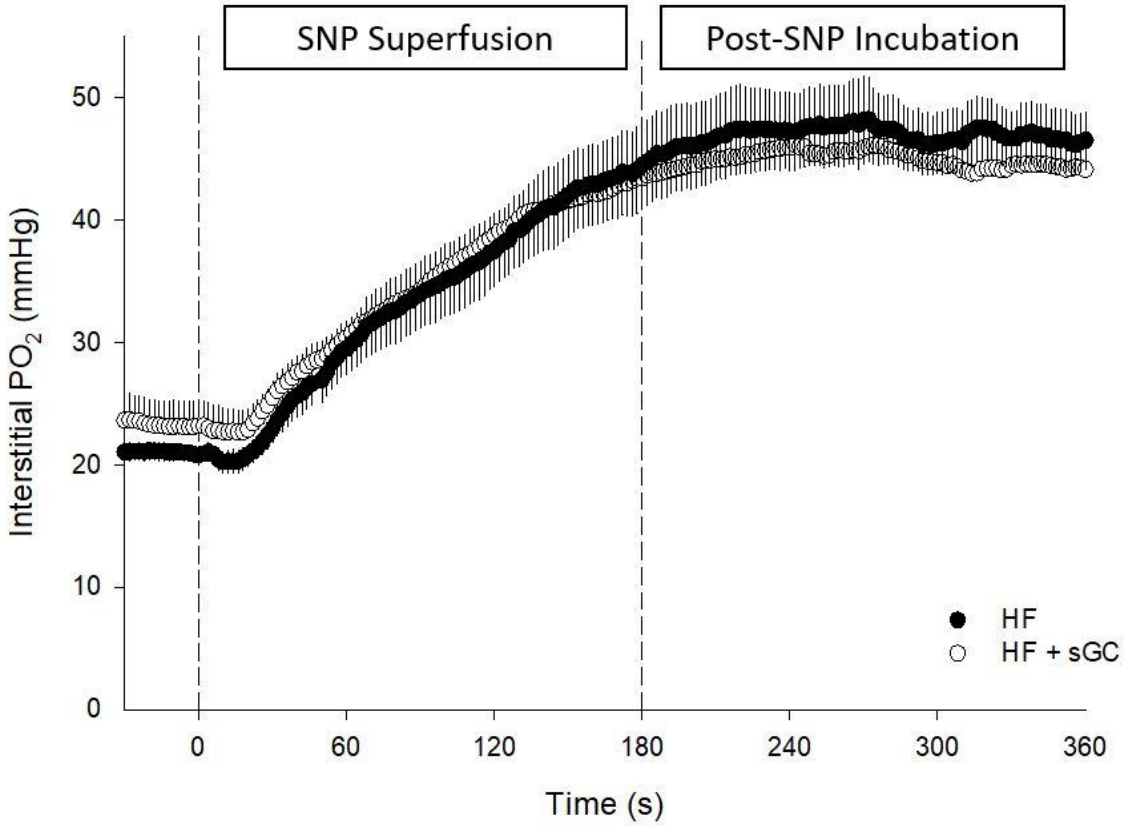

Figure 7: Effect of SNP superfusion on interstitial PO_2. Group mean (± SE) PO_2*is* dynamic profiles during 30 s of rest, 180 s of superfusion, and 180 s of incubation. Dashed lines indicate onset (0 s) and termination (180 s) of superfusion. Analyzed via two-way repeated measure ANOVA. $P > 0.05$ at all timepoints. HF; closed circles, HF + sGC; open circles.

Table 1: Morphometric data. Data are means ± SE. LV, left ventricle, SBP, systolic blood pressure; DBP, diastolic blood pressure; LVEDP, left ventricular end-diastolic pressure; +dP/dt, rise in blood pressure over time; RV, right ventricle, BW; body weight. Analyzed via unpaired student's t-test. * $P < 0.05$ vs HF.

	HF	HF + sGC
Infarct Size (%)	28 ± 3	29 ± 2
Heart rate (beats/min)	377 ± 10	346 ± 7 *
LVSBP (mmHg)	115 ± 3	109 ± 2
LVDBP (mmHg)	90 ± 3	78 ± 2 *
LVEDP (mmHg)	14 ± 1	16 ± 1
LV +dP/dT (mmHg/s)	8082 ± 264	7709 ± 397
LV/BW (mg/g)	2.00 ± 0.04	1.96 ± 0.07
RV/ BW (mg/g)	0.62 ± 0.04	0.62 ± 0.03
Lung/BW (mg/g)	3.17 ± 0.10	3.75 ± 0.12 *
Body Weight (g)	500 ± 12	454 ± 10 *

Table 2: Blood gas values. Values are means ± SE. Hct, hematocrit. Analyzed via unpaired student's t-test. * $P \leq 0.05$ vs. HF.

	HF	HF + sGC
pH	7.4 ± 0.0	7.4 ± 0.0
PCO_2 (mmHg)	31.1 ± 1.7	32.9 ± 1.1
PO_2 (mmHg)	87.2 ± 1.8	79.4 ± 7.4
% O_2 Sat	95.6 ± 0.4	95.8 ± 0.4
Hct (%)	34.2 ± 1.3	33.9 ± 3.0
Lactate (mmol/L)	1.3 ± 0.1	1.1 ± 0.1 *
Bicarbonate (mmol/L)	20.6 ± 0.9	21.7 ± 0.5
Base Excess (mmol/L)	-4.1 ± 0.8	-5.5 ± 2.7
Total CO_2 (mmol/L)	21.5 ± 0.9	22.8 ± 0.5

Table 3: Interstitial PO_2 kinetics parameters of spinotrapezius at rest and during 180 s of contractions in CON condition and following SNP superfusion. Values are means ± SE. $PO_{2(BL)}$, baseline interstitial PO_2; Δ1, PO_2 primary amplitude; τ, interstitial PO_2 value at timepoint of τ; TD, time delay, MRT, mean response time; PO_{2nadir}, nadir of PO_2 profile; Δ_2, secondary amplitude, $PO_{2(End)}$, interstitial PO_2 at end-contractions; AUC, area under the curve; $\Delta PO_2/\tau$, change in PO_2 for a given change in τ. Analyzed via two-way ANOVA. * $P < 0.001$ vs CON within group.

	CON		SNP	
	HF	**HF + sGC**	**HF**	**HF + sGC**
$PO_{2\,(BL)}$, mmHg	19.6 ± 1.0	23.3 ± 1.9	46.2 ± 2.8 *	44.0 ± 2.0 *
Δ_1, mmHg	13.3 ± 1.4	14.1 ± 1.8	23.4 ± 2.8 *	24.2 ± 1.9 *
τ, s	13 ± 1	13 ± 2	34 ± 4 *	38 ± 4 *
TD, s	8 ± 1	7 ± 1	8 ± 1	5 ± 2
MRT, s	21 ± 2	21 ± 3	42 ± 4 *	43 ± 5 *
$PO_{2(Nadir)}$, mmHg	6.3 ± 1.3	9.2 ± 1.2	22.8 ± 2.1 *	19.7 ± 1.8 *
Δ_2, mmHg	6.7 ± 1.7	7.8 ± 2.3	9.2 ± 4.4	3.1 ± 0.8
$PO_{2(End)}$, mmHg	13.0 ± 1.6	17.0 ± 2.2	32.0 ± 4.2 *	22.9 ± 1.6 *
AUC, mmHg	996 ± 123	1206 ± 114	2678 ± 172 *	2566 ± 215 *
$\Delta PO_2/\tau$, mmHg/s	1.0 ± 0.12	1.1 ± 0.2	0.8 ± 0.1	0.7 ± 0.1 *

Chapter 4 - Discussion

To our knowledge, this present investigation is the first to study the effects of sGC activation on capillary hemodynamics and PO_2*is* in the skeletal muscle of HF rats. Data herein support the hypothesis that chronic administration of a sGC activator improves $\dot{Q}O_2$-to-$\dot{V}O_2$ matching in skeletal muscle (PO_2*is*) of HF rats during twitch contractions due, in part, to increased capillaries supporting flow, f_{RBC}, V_{RBC}, and Hct_{cap} seen at rest. As previously demonstrated, there is a significant decrease in PO_2*is* (Craig et al., 2019a) and f_{RBC} and V_{RBC} (Kindig et al., 1999) in HF rats which likely contribute to the exercise intolerance characteristic of this diseased population. Taken together, these data demonstrate that the sGC activator effectively targets pathological and oxidized sGC thereby resulting in vasodilation, and thus improved $\dot{Q}O_2$-to-$\dot{V}O_2$ matching in the skeletal muscle of HF rats.

The rat model of HF provides a valuable model for assessing the central and peripheral dysfunction seen in clinical populations (Pfeffer et al., 1979; Musch, 1993). Importantly, the index of MI (% of endocardial surface area infarcted) and LVEDP were not different between groups (Table 1) and indicated moderate HF (Musch, 1993). In rats with a similar degree of HF, endothelial dysfunction occurs despite enhanced vascular eNOS and sGC expression, illustrating the ultimate effects of increased vascular ROS (Bauersachs & Widder, 2008).

Capillary hemodynamics in HF + sGC

Endothelial dysfunction and diminished skeletal muscle blood flow is due, in part, to decreased NO bioavailability via eNOS uncoupling, oxidative stress resulting in circulating ROS and ultimately sGC oxidation via ROS (Münzel et al., 2005). Determining the temporal and spatial distribution of RBCs, which is impaired in HF (Kindig et al., 1999, Richardson et al.,

2003), is imperative to understanding the effect of sGC activation on PO_2*is* and therefore blood-myocyte O_2 exchange. Importantly, capillary hemodynamics at rest in HF rats exhibit a decreased f_{RBC} and V_{RBC}, which has shown to improve with dietary nitrate (Ferguson et al., 2014). Therefore, we hypothesized that chronic administration of sGC activator would further increase the proportion of capillaries supporting flow and RBC dynamics (f_{RBC}, V_{RBC}, and Hct_{cap}).

Indeed, following sGC activator administration, more capillaries were supporting RBC flow and there was augmented f_{RBC} in those capillaries in the skeletal muscle of HF rats (Figure 1, Figure 3, Figure 5). Interestingly, we did not detect an elevated PO_2*is* at rest prior to contractions, but this may help describe the temporarily elevated PO_2*is* following contractions onset. SNP superfusion did not result in any differences between HF and HF + sGC groups. This does not correspond directly with the PO_2*is* data, where SNP superfusion increased PO_2*is*, indicating increased $\dot{Q}O_2$-to-$\dot{V}O_2$ matching at rest. One potential explanation resides in the spatial heterogeneity of $\dot{Q}O_2$ among individual fiber fields (Kindig et al., 1999, 2002, Poole et al., 1997), where it is possible to have an increased f_{RBC}, V_{RBC}, and Hct_{cap} in a smaller region of skeletal muscle, whereas changes in PO_2*is*, reflect a larger times sample that may sum many smaller regions with variable $\dot{Q}O_2$-to-$\dot{V}O_2$ ratios. It is possible that the elevated f_{RBC}, V_{RBC}, and Hct_{cap} in HF + sGC at rest may alleviate some of the $\dot{Q}O_2$-to-$\dot{V}O_2$ mismatch seen as metabolic demands increase (i.e. 14-22 seconds during contractions) (Figure 6A).

Interstitial $PO_2$is in HF

Skeletal muscle PO_2*is* kinetics reflect the dynamic matching between $\dot{Q}O_2$ and $\dot{V}O_2$ within the interstitial space during transitions in metabolic demand (Colburn et al., 2020; Craig et

al., 2019a; Craig et al., 2019b; Hirai et al., 2018). In health, following the onset of muscular contractions, there is a rapid increase in $\dot{Q}O_2$ to meet mitochondrial oxygen consumption (i.e., elevated $\dot{V}O_2$) (Kindig et al., 2002; Koga et al., 2014; Jones & Poole, 2005; Walsh et al., 2005), which elicits shear-stress mediated vasodilation in locomotory skeletal muscle (Luscher & Vanhoutte, 1990; Pohl et al., 1991; Lu & Kassab, 2011). However, peripheral derangements in rats with moderate HF compromise the f_{RBC} and V_{RBC} to the myocyte, thereby impairing diffusive and conductive O_2 delivery across the rest-to-contraction transition (Richardson et al., 2003), thus diminishing the PO_2 driving oxygen into the skeletal muscle. Notably, a more precipitous fall in PO_2*is* following the onset of contractions in HF, compared to health, is indicative of a slower rate of increase in $\dot{Q}O_2$-to-$\dot{V}O_2$. Endothelial dysfunction via local humoral components, namely decreased eNOS and NO bioavailability, contribute to these metabolic inefficiencies (Hirai et al., 1994; Copp et al., 2012). Prior studies from our laboratory indicate that five days of dietary nitrate supplementation in HF rats increased PO_2*is*, thereby enhancing $\dot{Q}O_2$-to-$\dot{V}O_2$ matching in the interstitial space (Craig et al., 2019b), potentially via increased percentage of capillaries supporting blood flow at rest and during contractions (Ferguson et al., 2014, 2016). Within the capillary bed, there is a vast surface area for O_2 exchange, but altered distribution of diminished bulk blood flow in HF limits $\dot{Q}O_2$-to-$\dot{V}O_2$ matching in skeletal muscles at rest (Kindig et al., 1999) and during exercise (Musch & Terrell, 1992).

Interstitial PO_2 in HF + sGC

sGC activators, which have been previously under-studied in skeletal muscle, can decrease progressive cardiac remodeling following MI (Irvine et al., 2012, Fraccarollo et al., 2014) and improve vascular smooth muscle function throughout the pulmonary vasculature

(Deruelle et al., 2005, Pankey et al., 2011). As such, much of the literature supporting sGC activators as a therapeutic in HF have focused on improving cardiac and pulmonary function (Irvine et al., 2012, Fraccarollo et al., 2014), yet, minimal research focuses on improving the peripheral vascular function in HF that ultimately contributes to exercise intolerance and handicaps effective exercise rehabilitation

In this investigation we demonstrate for the first time that chronic administration of sGC activator improves (i.e., elevates $PO_2$is) the PO_2*is* profile following the onset of contractions in the spinotrapezius muscle of HF rats during seconds 14-22, Figure 6A. During this time, augmented perfusive and diffusive delivery of O_2 conflate to raise PO_2*is* across the rest to exercise transition (Hirai et al., 2017; Colburn et al., 2020), thereby increasing the driving pressure of O_2 across the sarcolemma into the mitochondria. An increased PO_2*is* in HF + sGC compared to HF is expected to speed $V\dot{O}_2$ kinetics, thereby decreasing the O_2 deficit ($\dot{Q}O_2$-to-$\dot{V}O_2$ mismatch) and reliance upon anaerobic pathways for ATP regeneration; thereby supporting sustained exercise bouts by reducing intracellular metabolic perturbations that contribute to exhaustion (Poole et al., 2008; Richardson et al., 1998). Evidence supporting this notion, including the lower blood lactate concentration following twitch contractions in HF + sGC compared to HF, indicating either a reduced glycolysis during contractions or improved lactate removal (Massie et al., 1988; Drexler et al., 1992; Poole et al., 2012, 2020). Previous studies have shown accelerated glycolysis and glycogenolysis in response to an increased proportion and recruitment of type II fibers in HF (Sullivan et al., 1991; Drexler et al., 1992; Lipkin et al., 1988; Mancini et al., 1989). Therefore, it is likely that with a greater PO_2*is* during contractions and a decreased blood lactate production/increased removal, following treatment with the sGC

activator, HF patients may rely less on anaerobic energy production and potentially an increased time-to-fatigue during exercise.

It is well established that NO bioavailability is reduced in HF, therefore, exogenous NO-donors have proven to be beneficial in exercise (Craig et al., 2019b; Ferguson et al., 2013, Lundberg et al., 2011). However, oxidative stress seen in HF shifts intracellular levels of sGC towards the oxidized, dysfunctional, and heme-free form that is unresponsive to exogenous and endogenous NO (Nishiyama et al., 1998; Thoonen et al., 2015; Evgenov, et al., 2006). Therefore, in this investigation we sought to determine whether endothelium-independent sGC activation enhances $\dot{Q}O_2$-to-$\dot{V}O_2$ matching and whether exogenous NO (SNP) superfusion in addition to sGC activation would further improve skeletal muscle oxygenation. In response to SNP, there was no difference in PO_2*is* between HF and HF + sGC (Figure 6B, Figure 7, Table 3). However, SNP altered PO_2*is* kinetics vs. HF + sGC during CON conditions. As previously discussed, in our model of HF, herein, the MI% correlated with moderate HF (~30%) (Musch, 1993). Therefore, as oxidative stress increases with increased HF severity (Dhalla et al., 1996), sGC throughout the smooth muscle may not be completely oxidized, leaving sGC reduced and active in some portions of the vascular smooth muscle, explaining the presence of an acute effect of SNP.

Clinical Implications

Improving exercise tolerance in HF patients is an ongoing challenge. This study indicates that sGC activators may be beneficial to combating the exercise intolerance characteristic of HF patients by increasing skeletal muscle vasodilation via activation of oxidized sGC. Although this study utilizes single muscle twitch contractions, studies suggest targeting individual muscles or

muscle groups in patient populations can improve constant and peripheral perfusive and diffusive O_2 transport (Esposito et al., 2011).

With increased sodium retention, and thus increased fluid retention, the progression and severity of HF worsens. Interestingly, in HF, sGC activators (via increases in cGMP) have recently been shown to decrease sympathetic outflow and increase renal perfusion (Frees et al., 2020). In the current study, there was a decreased BW with HF + sGC compared to HF. The lower BW with HF + sGC suggests that sGC activators may decrease sodium retention and subsequently fluid retention in HF. Thus, sGC activators highlight a potential therapeutic avenue to ameliorate the progression of HF.

Experimental Considerations

This study only assessed the mode of action of sGC activators in male rats. Women have a lower prospect of developing heart disease until they are postmenopausal, where the incidence increases dramatically. Recently, data suggests that women rely on greater basal NO bioavailability in HF (Craig et al., 2019b). Therefore, future studies warrant investigating PO_2*is* and capillary hemodynamics in female rats and ovariectomized female rats receiving sGC activator. Assessing capillary hemodynamics presents challenges, regarding small sampling area/volume and variability among sampled fields. These were overcome by using careful and precise techniques on several frames per muscle to limit errors in assessing capillary hemodynamics. Furthermore, multiple investigators were involved in analysis, thereby increasing scientific rigor. Lastly, sGC activators are only capable of activating the oxidized heme on sGC, therefore, in order to assess the entirety of its effects in the microcirculation, a

larger MI%, resulting in greater increases in ROS (i.e., more pathological sGC), is necessary in order to assess the utility of sGC activators across a range of HF severity.

Conclusions

This study is the first to demonstrate the efficacy of chronic administration of sGC activators in HF in the muscle microcirculation and its ability to modulate $\dot{Q}O_2$ relative to $\dot{V}O_2$ at rest and during submaximal electrically-induced contractions. Specifically, at rest the sGC activator increased the proportion of capillaries supporting flow, f_{RBC}, V_{RBC}, and Hct_{cap} compared to HF. Increased PO_2*is* during contractions suggests improved $\dot{Q}O_2$-to-$\dot{V}O_2$ matching during submaximal exercise. The increases in both perfusive and diffusive measures of O_2 transport in HF + sGC have significant implications for potential therapeutics targeting the oxidized sGC seen in HF which may improve exercise tolerance and decrease mortality and morbidity.

References

1. Abraham, W. T., Fisher, W. G., Smith, A. L., Delurgio, D. B., Leon, A. R., Loh, E., Kocovic, D., Packer, M., Clavell, A., Hayes, D., Ellestad, M., & Trupp, R. (2002). Cardiac resynchronization in chronic heart failure. New England Journal of Medicine, 346(24), 1845-1853.
2. Altman PL and Dittmer DS. Biology Data Book (2nd ed.). Bethesda, MD: FASEB, 1974, p. 1598–1613.
3. Bailey, JK, Kindig CA, Behnke BJ, Musch TI, Schmid-Schoenbein GW, Poole DC. Spinotrapezius muscle microcirculatory function: effects of surgical exteriorization. *Am J Physiol Heart Circ Physiol* 279: H3131-H3137, 2000.
4. Bauersachs, J., & Widder, J. D. (2008). Endothelial dysfunction in heart failure. Pharmacological reports, 60(1), 119.
5. Behnke, B. J., Barstow, T. J., Kindig, C. A., McDonough, P., Musch, T. I., & Poole, D. C. (2002). Dynamics of oxygen uptake following exercise onset in rat skeletal muscle. *Respiratory physiology & neurobiology*, *133*(3), 229-239.
6. Benz, K., Orth, S. R., Simonaviciene, A., Linz, W., Schindler, U., Rütten, H., & Amann, K. (2007). Blood pressure-independent effect of long-term treatment with the soluble heme-independent guanylyl cyclase activator HMR1766 on progression in a model of noninflammatory chronic renal damage. Kidney and Blood Pressure Research, 30(4), 224-233.
7. Brunton, T. L. (1897). The relationship of physiology, pharmacology, pathology and practical medicine. Nature, 56(473), 187.

8. Butler, J., Yang, M., Manzi, M. A., Hess, G. P., Patel, M. J., Rhodes, T., & Givertz, M. M. (2019). Clinical course of patients with worsening heart failure with reduced ejection fraction. Journal of the American College of Cardiology, 73(8), 935-944.
9. Cai, H., & Harrison, D. G. (2000). Endothelial dysfunction in cardiovascular diseases: the role of oxidant stress. Circulation research, 87(10), 840-844.
10. Colburn, T. D., Hirai, D. M., Craig, J. C., Ferguson, S. K., Weber, R. E., Schulze, K. M., Behnke, B. J., Musch, T. I., & Poole, D. C. (2020). Transcapillary PO2 Gradients in contracting muscles across the fibre type and oxidative continuum. *The Journal of Physiology*.
11. Copp, S. W., Hirai, D. M., Ferguson, S. K., Holdsworth, C. T., Musch, T. I., & Poole, D. C. (2012). Effects of chronic heart failure on neuronal nitric oxide synthase-mediated control of microvascular O2 pressure in contracting rat skeletal muscle. The Journal of physiology, 590(15), 3585-3596.
12. Craig JC, Colburn TD, Caldwell JT, Hirai DM, Tabuchi A, Baumfalk DR, Behnke BJ, Ade CJ, Musch TI, Poole DC. (2019a) Central and peripheral factors mechanistically linked to exercise intolerance in heart failure with reduced ejection fraction. Am J Physiol Heart Circ Physiol. 2019 Aug 1;317(2):H434-H444. doi: 10.1152/ajpheart.00164.2019.
13. Craig, J. C., Colburn, T. D., Hirai, D. M., Musch, T. I., & Poole, D. C. (2019b). Sexual dimorphism in the control of skeletal muscle interstitial Po2 of heart failure rats: effects of dietary nitrate supplementation. *Journal of Applied Physiology*, *126*(5), 1184-1192.

14. Daiber, A., & Münzel, T. (2015). Organic nitrate therapy, nitrate tolerance, and nitrate-induced endothelial dysfunction: emphasis on redox biology and oxidative stress. Antioxidants & redox signaling, 23(11), 899-942.
15. Delp, M. D., & Duan, C. (1996). Composition and size of type I, IIA, IID/X, and IIB fibers and citrate synthase activity of rat muscle. Journal of applied physiology, 80(1), 261-270.
16. Deruelle, P., Grover, T. R., Storme, L., & Abman, S. H. (2005). Effects of BAY 41–2272, a soluble guanylate cyclase activator, on pulmonary vascular reactivity in the ovine fetus. American Journal of Physiology-Lung Cellular and Molecular Physiology, 288(4), L727-L733
17. Dhalla, A. K., Hill, M. F., & Singal, P. K. (1996). Role of oxidative stress in transition of hypertrophy to heart failure. Journal of the American College of Cardiology, 28(2), 506-514.
18. Diederich, E. R., Behnke, B. J., McDonough, P., Kindig, C. A., Barstow, T. J., Poole, D. C., & Musch, T. I. (2002). Dynamics of microvascular oxygen partial pressure in contracting skeletal muscle of rats with chronic heart failure. Cardiovascular research, 56(3), 479-486.
19. Drexler, H., Riede, U., Münzel, T., König, H., Funke, E., & Just, H. (1992a). Alterations of skeletal muscle in chronic heart failure. Circulation, 85(5), 1751-1759.
20. Drexler, H., Hayoz, D., Münzel, T., Hornig, B., Just, H., Brunner, H. R., & Zelis, R. (1992b). Endothelial function in chronic congestive heart failure. American Journal of Cardiology, 69(19), 1596-1601.

21. Elkayam, S., Kulick, D., McIntosh, N, Roth, A.., Hsueh, W., & Rahimtoola, S. H. (1987). Incidence of early tolerance to hemodynamic effects of continuous infusion of nitroglycerin in patients with coronary artery disease and heart failure. *Circulation*, *76*(3), 577-584.
22. Esipova, T. V., Karagodov, A., Miller, J., Wilson, D. F., Busch, T. M., & Vinogradov, S. A. (2011). Two new "protected" oxyphors for biological oximetry: properties and application in tumor imaging. Analytical chemistry, 83(22), 8756-8765.
23. Esposito, F., Reese, V., Shabetai, R., Wagner, P. D., & Richardson, R. S. (2011). Isolated quadriceps training increases maximal exercise capacity in chronic heart failure: the role of skeletal muscle convective and diffusive oxygen transport. Journal of the American College of Cardiology, 58(13), 1353-1362.
24. Evgenov, O. V., Pacher, P., Schmidt, P. M., Haskó, G., Schmidt, H. H., & Stasch, J. P. (2006). NO-independent stimulators and activators of soluble guanylate cyclase: discovery and therapeutic potential. Nature reviews Drug discovery, 5(9), 755-768.
25. Federspiel, W. J., & Popel, A. S. (1986). A theoretical analysis of the effect of the particulate nature of blood on oxygen release in capillaries. Microvascular research, 32(2), 164-189.
26. Ferguson, S. K., Hirai, D. M., Copp, S. W., Holdsworth, C. T., Allen, J. D., Jones, A. M., ... & Poole, D. C. (2013). Impact of dietary nitrate supplementation via beetroot juice on exercising muscle vascular control in rats. The Journal of physiology, 591(2), 547-557.

27. Ferguson, S., Holdsworth, C., Wright, J., Fees, A., Musch, T., & Poole, D. (2014). Impact of nitrate supplementation via beetroot juice on capillary hemodynamics in skeletal muscle of rats in chronic heart failure (1106.16). The FASEB Journal, 28(1_supplement), 1106-16.
28. Ferguson, S. K., Holdsworth, C. T., Colburn, T. D., Wright, J. L., Craig, J. C., Fees, A., Jones, A., Allen, J., Musch, T., & Poole, D. C. (2016). Dietary nitrate supplementation: impact on skeletal muscle vascular control in exercising rats with chronic heart failure. *Journal of applied physiology*, *121*(3), 661-669.
29. Ferreira, L. F., McDonough, P., Behnke, B. J., Musch, T. I., & Poole, D. C. (2006). Blood flow and O2 extraction as a function of O2 uptake in muscles composed of different fiber types. Respiratory physiology & neurobiology, 153(3), 237-249.
30. Frees, A., Assersen, K. B., Jensen, M., Hansen, P. B., Vanhoutte, P. M., Madsen, K., Federlein A., Lund L., Toft A. & Jensen, B. L. (2020). Natriuretic peptides relax human intrarenal arteries through natriuretic peptide receptor type-A recapitulated by soluble guanylyl cyclase agonists. Acta Physiologica, e13565.
31. Fraccarollo, D., Galuppo, P., Motschenbacher, S., Ruetten, H., Schäfer, A., & Bauersachs, J. (2014). Soluble guanylyl cyclase activation improves progressive cardiac remodeling and failure after myocardial infarction. Cardioprotection over ACE inhibition. Basic research in cardiology, 109(4), 421.
32. Hillege, H. L., Girbes, A. R., De Kam, P. J., Boomsma, F., De Zeeuw, D., Charlesworth, A., Hampton, J., & Van Veldhuisen, D. J. (2000). Renal function, neurohormonal activation, and survival in patients with chronic heart failure. Circulation, 102(2), 203-210.

33. Hirai, D. M., Zelt, J. T., Jones, J. H., Castanhas, L. G., Bentley, R. F., Earle, W., Staples, P., Tschakovsky, M., McCans, J., O'Donnell, D., & Neder, J. A. (2017). Dietary nitrate supplementation and exercise tolerance in patients with heart failure with reduced ejection fraction. American Journal of Physiology-Regulatory, Integrative and Comparative Physiology, 312(1), R13-R22.

34. Hirai DM, Craig JC, Colburn TD, Eshima H, Kano Y, Sexton WL, Musch TI, Poole DC. (2018). Skeletal muscle microvascular and interstitial PO2 from rest to contractions. J Physiol. 2018 Mar 1;596(5):869-883. doi: 10.1113/JP275170. Epub 2018 Jan 30. PMID: 29288568; PMCID: PMC5830449.

35. Hirai, D. M., Colburn, T. D., Craig, J. C., Hotta, K., Kano, Y., Musch, T. I., & Poole, D. C. (2019). Skeletal muscle interstitial O2 pressures: Bridging the gap between the capillary and myocyte. Microcirculation, 26(5), e12497.

36. Hirai, T., Visneski, M. D., Kearns, K. J., Zelis, R., & Musch, T. I. (1994). Effects of NO synthase inhibition on the muscular blood flow response to treadmill exercise in rats. Journal of applied physiology, 77(3), 1288-1293.

37. Hirai, T., Zelis, R., & Musch, T. I. (1995). Effects of nitric oxide synthase inhibition on the muscle blood flow response to exercise in rats with heart failure. Cardiovascular research, 30(3), 469-476.

38. Irvine, J. C., Ganthavee, V., Love, J. E., Alexander, A. E., Horowitz, J. D., Stasch, J. P., Kemp-Harper, B. K., & Ritchie, R. H. (2012). The soluble guanylyl cyclase activator bay 58-2667 selectively limits cardiomyocyte hypertrophy. PloS one, 7(11), e44481.

39. Jones, A. M. & Poole, D. C. (2005). Oxygen uptake dynamics: from muscle to mouth—an introduction to the symposium. Medicine & Science in Sports & Exercise, 37(9), 1542-1550.

40. Kindig CA, Sexton WL, Fedde MR, and Poole DC. (1998). Skeletal muscle microcirculatory structure and hemodynamics in diabetes. Respir Physiol 111: 163–175.

41. Kindig, C. A., Musch, T. I., Basaraba, R. J., & Poole, D. C. (1999). Impaired capillary hemodynamics in skeletal muscle of rats in chronic heart failure. Journal of applied physiology, 87(2), 652-660.

42. Kindig, C. A., Richardson, T. E., & Poole, D. C. (2002). Skeletal muscle capillary hemodynamics from rest to contractions: implications for oxygen transfer. Journal of applied physiology, 92(6), 2513-2520.

43. Knorr A, Hirth-Dietrich C, Alonso-Alija C, Härter M, Hahn M, Keim Y, Wunder F, Stasch JP. Nitric oxide-independent activation of soluble guanylate cyclase by BAY 60-2770 in experimental liver fibrosis. Arzneimittelforschung. 2008;58(2):71-80. doi: 10.1055/s-0031-1296471. PMID: 18412020.

44. Koga, S., Rossiter, H. B., Heinonen, I., Musch, T. I., & Poole, D. C. (2014). Dynamic heterogeneity of exercising muscle blood flow and O2 utilization. Medicine and science in sports and exercise, 46(5), 860.

45. La Rovere, M. T., Pinna, G. D., Maestri, R., Mortara, A., Capomolla, S., Febo, O., Ferrari, R., Franchini, M., Gnemmi, M., Opasich, C., Riccardi, P. G., Traversi, E., & Cobelli, F. (2003). Short-term heart rate variability strongly predicts sudden cardiac death in chronic heart failure patients. circulation, 107(4), 565-570.

46. Lipkin, D. P., Jones, D. A., Round, J. M., & Poole-Wilson, P. A. (1988). Abnormalities of skeletal muscle in patients with chronic heart failure. International journal of cardiology, 18(2), 187-195.

47. Lu, D., & Kassab, G. S. (2011). Role of shear stress and stretch in vascular mechanobiology. Journal of the royal society interface, 8(63), 1379-1385.

48. Lundberg, J. O., Carlström, M., Larsen, F. J., & Weitzberg, E. (2011). Roles of dietary inorganic nitrate in cardiovascular health and disease. Cardiovascular research, 89(3), 525-532.

49. Luscher TF, Vanhoutte PM. The Endothelium:Modulator of Cardiovascular Function. Boca Raton, FL: CRC Press, 1990, p. 1-162.

50. Massie, B. M., Conway, M., Rajagopalan, B., Yonge, R., Frostick, S., Ledingham, J., Sleight, P., & Radda, G. (1988). Skeletal muscle metabolism during exercise under ischemic conditions in congestive heart failure. Evidence for abnormalities unrelated to blood flow. Circulation, 78(2), 320-326.

51. Mancini, D. M., Coyle, E., Coggan, A., Beltz, J., Ferraro, N., Montain, S., & Wilson, J. R. (1989). Contribution of intrinsic skeletal muscle changes to 31P NMR skeletal muscle metabolic abnormalities in patients with chronic heart failure. Circulation, 80(5), 1338-1346.

52. Münzel, T., Daiber, A., Ullrich, V., & Mülsch, A. (2005). Vascular consequences of endothelial nitric oxide synthase uncoupling for the activity and expression of the soluble guanylyl cyclase and the cGMP-dependent protein kinase. Arteriosclerosis, thrombosis, and vascular biology, 25(8), 1551-1557.

53. Münzel, T., Daiber, A., & Mülsch, A. (2005). Explaining the phenomenon of nitrate tolerance. Circulation research, 97(7), 618-628.

54. Münzel, T., Daiber, A., & Gori, T. (2011). Nitrate therapy: new aspects concerning molecular action and tolerance. Circulation, 123(19), 2132-2144.

55. Musch, T. I., & Terrell, J. A. (1992). Skeletal muscle blood flow abnormalities in rats with a chronic myocardial infarction: rest and exercise. American Journal of Physiology-Heart and Circulatory Physiology, 262(2), H411-H419.

56. Nishiyama, Y., Ikeda, H., Haramaki, N., Yoshida, N., & Imaizumi, T. (1998). Oxidative stress is related to exercise intolerance in patients with heart failure. American heart journal, 135(1), 115-120.

57. Pankey EA, Bhartiya M, Badejo AM Jr, et al. Pulmonary and systemic vasodilator responses to the soluble guanylyl cyclase activator, BAY 60-2770, are not dependent on endogenous nitric oxide or reduced heme. American Journal of physiology. Heart and Circulatory Physiology. 2011 Mar;300(3):H792-802. DOI: 10.1152/ajpheart.00953.2010

58. Pfeffer, M. A., Pfeffer, J. M., Fishbein, M. C., Fletcher, P. J., Spadaro, J., Kloner, R. A., & Braunwald, E. (1979). Myocardial infarct size and ventricular function in rats. *Circulation research*, *44*(4), 503-512.

59. Piepoli, M. F., & Crisafulli, A. (2014). Pathophysiology of human heart failure: importance of skeletal muscle myopathy and reflexes. Experimental physiology, 99(4), 609-615.

60. Pohl U, Herlan K, Huang A, Bassenge E. EDRF-mediated shear induced dilation opposes myogenic vasoconstriction in small rabbit arteries. Am J Physiol Heart Circ Physiol 261: H2016-H2023, 1991.
61. Poole, D. C., Musch, T. I., & Kindig, C. A. (1997). In vivo microvascular structural and functional consequences of muscle length changes. American Journal of Physiology-Heart and Circulatory Physiology, 272(5), H2107-H2114.
62. Poole, D. C., Barstow, T. J., McDonough, P., & Jones, A. M. (2008). Control of oxygen uptake during exercise. Medicine and science in sports and exercise, 40(3), 462-474.
63. Poole, D. C., Hirai, D. M., Copp, S. W., & Musch, T. I. (2012). Muscle oxygen transport and utilization in heart failure: implications for exercise (in) tolerance. American Journal of Physiology-Heart and Circulatory Physiology, 302(5), H1050-H1063.
64. Poole, D. C., Richardson, R. S., Haykowsky, M. J., Hirai, D. M., & Musch, T. I. (2018). Exercise limitations in heart failure with reduced and preserved ejection fraction. Journal of applied physiology, 124(1), 208-224.
65. Richardson, R. S., Noyszewski, E. A., Leigh, J. S., & Wagner, P. D. (1998). Lactate efflux from exercising human skeletal muscle: role of intracellular PO 2. Journal of Applied Physiology, 85(2), 627-634.
66. Richardson, T. E., Kindig, C. A., Musch, T. I., & Poole, D. C. (2003). Effects of chronic heart failure on skeletal muscle capillary hemodynamics at rest and during contractions. Journal of Applied Physiology, 95(3), 1055-1062.

67. Silva, F. H., Leiria, L. O., Alexandre, E. C., Davel, A. P. C., Mónica, F. Z., De Nucci, G., & Antunes, E. (2014). Prolonged therapy with the soluble guanylyl cyclase activator BAY 60-2770 restores the erectile function in obese mice. The Journal of Sexual Medicine, 11(11), 2661-2670.

68. Stone, J. R., & Marletta, M. A. (1994). Soluble guanylate cyclase from bovine lung: activation with nitric oxide and carbon monoxide and spectral characterization of the ferrous and ferric states. *Biochemistry*, *33*(18), 5636-5640.

69. Stasch JP, Schmidt PM, Nedvetsky PI, Nedvetskaya TY, H S AK, Meurer S, Deile M, Taye A, Knorr A, Lapp H, Müller H, Turgay Y, Rothkegel C, Tersteegen A, Kemp-Harper B, Müller-Esterl W, Schmidt HH. Targeting the heme-oxidized nitric oxide receptor for selective vasodilatation of diseased blood vessels. J Clin Invest. 2006 Sep;116(9):2552-61. doi: 10.1172/JCI28371. PMID: 16955146; PMCID: PMC1555649.

70. Sullivan, M. J., Green, H. J., & Cobb, F. R. (1991). Altered skeletal muscle metabolic response to exercise in chronic heart failure. Relation to skeletal muscle aerobic enzyme activity. Circulation, 84(4), 1597-1607.

71. Thoonen R, Cauwels A, Decaluwe K, Geschka S, Tainsh RE, Delanghe J, Hochepied T, De Cauwer L, Rogge E, Voet S, Sips P, Karas RH, Bloch KD, Vuylsteke M, Stasch JP, Van de Voorde J, Buys ES, Brouckaert P. Cardiovascular and pharmacological implications of haem-deficient NO-unresponsive soluble guanylate cyclase knock-in mice. Nat Commun. 2015 Oct 7;6:8482. doi: 10.1038/ncomms9482. PMID: 26442659; PMCID: PMC4699393.

72. Walsh, B., Howlett, R., Stary, C., Kindig, C., & Hogan, M. (2005). Determinants of oxidative phosphorylation onset kinetics in isolated myocytes. Medicine & Science in Sports & Exercise, 37(9), 1551-1558.

73. Warnholtz, A., Mollnau, H., Heitzer, T., Kontush, A., Möller-Bertram, T., Lavall, D., Giaid, A., Beisiegel, U., Marklund, S., Walkter, U., Munzel, T., & Meinertz, T. (2002). Adverse effects of nitroglycerin treatment on endothelial function, vascular nitrotyrosine levels and cGMP-dependent protein kinase activity in hyperlipidemic Watanabe rabbits. *Journal of the American College of Cardiology*, *40*(7), 1356-1363.